COUPON SCALE MODELLING OF THE BRIDGING MECHANICS OF HIGH-RATE LOADED Z-PINS

Bing Zhang[1], Antonio R. Melro[2], Ivana K. Partridge[3] and Stephen R. Hallett[4]

Bristol Composites Institute (ACCIS), University of Bristol, Queen's Building, University Walk, Bristol BS8 1TR, UK
[1]Email: b.zhang@bristol.ac.uk,
Web Page: http://www.bristol.ac.uk/engineering/people/bing-zhang/index.html
[2]Email: antonio.melro@bristol.ac.uk,
Web Page: http://www.bristol.ac.uk/engineering/people/antonio-r-melro/index.html
[3]Email: Ivana.Partridge@bristol.ac.uk,
Web Page: http://www.bristol.ac.uk/engineering/people/ivana-k-partridge/index.html
[4]Email: Stephen.Hallett@bristol.ac.uk,
Web Page: http://www.bristol.ac.uk/engineering/people/stephen-r-hallett/index.html

Keywords: laminates, delamination, z-pinning, mechanical properties, Finite element analysis (FEA)

Abstract

This work presents an advanced finite element model that can be used to investigate and understand the high-loading-rate bridging mechanisms of z-pins. Ply-by-ply meshes are used to consider the microstructure of a z-pin array reinforced laminate, with the pin and resin pocket explicitly modelled. The resin is described by an elasto-plastic model that is dependent on both hydrostatic pressure and on the loading rate. The interface between the z-pin and the laminate is described by a coupled cohesive and friction contact algorithm; a friction term is added on top of Coulomb friction to consider the roughness of the z-pin and hole surfaces, which are difficult to mesh directly in the finite element model. To improve computational efficiency, each z-pin is described without progressive damage and a nonlinear shear constitutive law is used to account for the variation of z-pin bending stiffness due to splitting. Rupture of z-pins is described by the maximum tensile stress criterion with the tensile strength described by a Weibull criterion. The model was preliminarily applied to simulate the mode I high-rate bridging behaviour of a 4 × 4 z-pin array inserted in a quasi-isotropic laminate. The numerical model has successfully captured z-pin/laminate debonding and frictional pullout.

1. Introduction

Ply separation consequent on mechanical loading of a cured laminated composite has always been a major concern for engineers. Recent decades have witnessed significant advance of through-thickness reinforcement (TTR) technologies, for example, stitching, 3D weaving and more recently tufting [1].

Inserting small diameter rods (z-pins) in the thickness direction of composite laminates has been proved to be a very effective technique for increasing delamination resistance. Most of the literature research on z-pinning has been focused on the quasi-static bridging capabilities of z-pins. However, impacts due to bird strike, tool drop, hail, etc., which would benefit from the application of z-pinning for delamination suppression, are usually high loading-rate scenarios. Thus, it becomes imperative to investigate the bridging mechanisms of z-pins under high-rate loading. Schlueter [2] investigated the loading rate effects on mode I delamination of z-pinned Double Cantilever Beams (DCBs) using a flying wedge test method. A wide range of wedge velocities were considered, including ~0 m/s (quasi-static), 0.5 m/s, 1.0 m/s, 3.3 m/s, 25 m/s, 40 m/s and 50 m/s. Experimental data showed that

both the critical peak crack closure traction exerted by z-pins and the apparent fracture toughness decreased with the wedge velocity up to 40 m/s. Zhang et al. [3] presented an experimental study on the bridging capability of circular z-pins when inserted in a pristine laminate plate under low-velocity impact (a mode II dominated case) in a narrow velocity range (from 1.65 m/s to 2.91 m/s). The presence of z-pins decreased the projected damage area, although it showed negative effects on the critical force corresponding to delamination onset. The specific effect of z-pins on damage area varies due to the specimen thickness and the impact energy. Given a z-pin areal density, Knaupp et al [4] found that rectangular z-pins offer better delamination suppression performance than circular z-pins through experimental test in a narrow range of velocities (from 1.89 m/s to 3.27 m/s). This is mainly due to the z-pin/laminate interface area of a rectangular pin is larger than a circular pin for the same pinning areal density. Yasaee et al. [5] presented experimental characterisation of z-pinned laminates through three-point End Notched Flexure (3ENF) specimens under quasi-static, 1 m/s, 3 m/s and 5.35 m/s displacement loading rates. It was concluded that the z-pinned specimens showed a significant increase in the apparent fracture toughness with loading rate. More recently, Cui et al. [6][7] characterised the dynamic bridging mechanisms of T300/BMI composite z-pins in the full range of mode mixity via laminate blocks that are separated by a release film at the mid-plane and bridged only by z-pins under the pullout velocities of ~ 0 m/s and 6 m/s. It was found that the z-pins showed decreasing bridging capability with loading rate in mode I dominated cases, which is mainly down to the rate sensitive frictional pullout stage. On the other hand, z-pins demonstrated comparable bridging capability between dynamic and quasi-static loading for mode II dominated cases.

This work presents the development of an advanced finite elemet model that can be used to investigate the high-loading-rate bridging mechanisms of composite z-pins. The model results are then compared against the experimental data presented in [6].

2. Modelling strategy

This section introduces the critical features of the modelling strategy, including numerical description of resin pockets and fibre waviness regions, ply-level meshes, z-pin/laminate interface and z-pin failure.

2.1. Resin pocket and fibre waviness region

The presence of a z-pin introduces a resin pocket and fibre waviness regions around the TTR element [1]. The profile of the resin pocket is described by a cosine function:

$$. |y| - 0.25 \cdot W_{RP} \cdot \left(\cos\left(\frac{2\pi|x|}{L}\right) + 1\right) = 0 \quad (1)$$

where L indicates the total resin pocket length, while W_{RP} indicates the maximum resin pocket width. This equation assures the zero fibre curvature at the resin pocket tip, which, however, was not considered by the previous equation in [8]. The function is defined in the local in-plane coordinate system of a z-pin; its origin is the centre of the z-pin; x-axis follows the global fibre orientation. In a z-pin array reinforced laminate, two adjacent resin pockets may merge into one resin channel when the pin to pin distance is smaller than the resin-pocket length and the two z-pins are not misaligned significantly in the local x-axis. The resin channel profile in the overlay region of the two resin pockets is simply assumed to be the sum of the two resin pocket profiles (Fig. 1). The mechanical behaviour of the resin pocket is described by an advanced constitutive model that combines the hydrostatic pressure dependent constitutive law developed by Melro et al. in [9] and the strain rate dependent constitutive law developed by Bai et al. in [10].

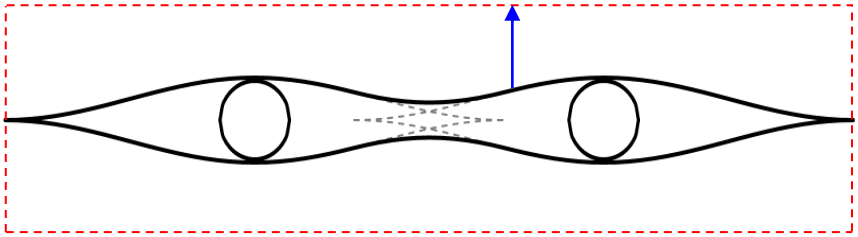

Figure 1. Numerical description of two joined resin pockets; dashed black lines indicate the individual resin pocket profile without overlay; dashed red lines indicate the fibre waviness region around the resin channel; an blue arrow line indicates a reference line used to define the fibre waviness angle.

The presence of z-pins will also introduce a fibre waviness region, which is assumed to be rectangular above and below the resin pocket/channel, as shown in Fig. 1. The fibre waviness region has the same length as the resin pocket and a width of *W*. The fibre waviness angle is assumed to decrease linearly from the inner boundary to the outer boundary along the lines in the local y-axis, one which is marked by a blue line in Fig. 1. The reference fibre waviness angle on the inner boundary of the fibre waviness region can be derived by Eq. 1, while the fibre waviness angle is zero on the outer edges of the fibre waviness region. Fibre volume fraction is expected to show the maximum (VF_{max}) at the top and bottom tips of the resin-pocket/laminate interface. On the outer boundary of the fibre waviness region, the fibre volume fraction is not affected by the presence of z-pins, thus equaling the nominal value of the laminate without TTR, VF_0. The fibre volume fraction in the fibre waviness region is defined by Eq. 2. In the case where two z-pins are close, the fibre volume fraction at a location is assumed to be the sum of the two values that are computed by treating each z-pin using Eq. 2 separately.

$$VF = VF_0 + \frac{4(VF_{max} - VF_0)}{W \cdot L}\left(\frac{L}{2} - |x|\right)\left(\frac{W}{2} - |y|\right) \quad (2)$$

2.2. Ply-level mesh

Based on the numerical descriptions regarding the typical microstructures of z-pinned laminates, it is straightforward to discretise a ply of a z-pinned laminate using finite elements. Fig. 2 shows a group of ply-level meshes which are used for the case study in Section 3. Figs. 2a-d are for 4 × 4 z-pin array ply-level meshes for the most commonly used ply orientations, i.e. -45°, 0°, +45° and 90°. These ply-level meshes show different node arrangement, thus a 'tie' constraint needs to be defined between two plies with different orientations to link the degrees of freedom (DOFs) between the surface pairs. Previous work presented a versatile ply-level mesh to avoid the 'tie' definition [8], however, it requires a much finer mesh to allow describing four differently oriented potential resin pockets in a quasi-isotropic laminate, which significantly increases computational effort, especially for z-pin array modelling.

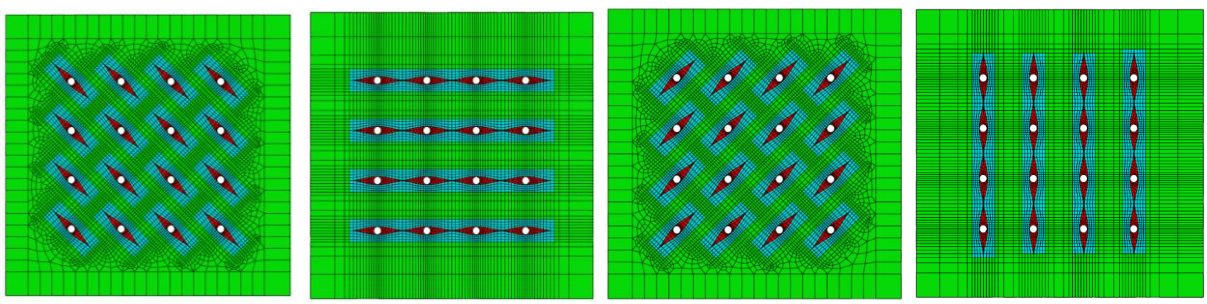

(a) (b) (c) (d)

Figure 2. z-pin array ply-level meshes for (a) -45°, (b) 0°, (c) 45° and (d) 90° plies.

2.3. Z-pin/laminate interface

The z-pin/laminate interface is governed by the combination of interface bonding and frictional contact between exposed surfaces. A cohesion-friction contact formulation has been proposed in [11] to describe the z-pin/laminate interface under static loading. It is here extended to high loading-rate cases. The interface model was developed based on the idea [12] that decomposes an interface into undamaged and damaged parts; the undamaged part deforms elastically while the damaged part is governed by a modified Coulomb friction law. The modified Coulomb friction law, similar to the ones used in [8] and [13], adds an additional friction term on top of standard Coulomb friction law, as expressed by:

$$\tau_F = \mu \cdot \sigma_F + \varphi \tag{3}$$

$$\varphi = \tau_0 \cdot \left(1 - \left(\frac{\max(0,\delta_I)}{\delta_0}\right)^5\right) \tag{4}$$

where σ_F indicates the normal pressure of the interface; μ is the Coulomb friction coefficient. The friction term φ is introduced to account for the sliding resistance due to the large geometrical irregularities and roughness of the exposed z-pin and hole surfaces, especially for the latter. The friction term φ allows applying friction even without the normal pressure. The non-pressure associated friction component is assumed to show the maximum τ_0 when pressure exists (i.e. $\delta_I \leq 0$) and starts decreasing from τ_0 to zero at the point when the interface is separated by a distance of δ_0. This cohesive-friction law activates friction following damage initiation of the interface, instead of following the full failure of the interface as assumed in Ref. [8].

2.4. Z-pin failure

A composite z-pin, standardly made by a putrusion process from T330/BMI , features two main failure mechanisms: inter-fibre debonding (splitting) and fibre breakage. A straightforward way to consider the splitting and subsequent friction mechanisms is inserting cohesive elements in potential locations (for splitting prediction) in combination of defining frictional contact between exposed surfaces after failure of the cohesive elements (for frictional contact between split strands) [8]. The approach has been proved to be capable of providing satisfactory prediction regarding the global bridging load versus displacement curves, although the predefined positions and number of splits may differ from experimental observations. To improve computational efficiency especially for z-pin array modelling, a more efficient way is used here. It describes a composite z-pin using a homogenised mesh in combination with a nonlinear constitutive equation for the axial shear stress versus strain relations. The main purpose of the nonlinear shear definition is to tailor the flexural modulus of the z-pin to account for the effect of splitting. A similar treatment was used in [14] and [15]. The nonlinear shear constitutive equation is expressed as:

$$\tau_{1i} = A \cdot sgn(\gamma_{1i}) \cdot \left(1 - e^{-B|\gamma_{1i}|}\right), \qquad i = 2,3 \tag{5}$$

where τ_{1i} indicates axial shear stresses, while γ_{1i} indicates axial shear strains. The controlling parameters A and B can be calibrated by fitting experimental data. Unloading is linearly controlled by the initial stiffness. This nonlinear shear constitutive equation was used for in-plane shear behaviour of composite laminates [16], and it is here extended to be used for z-pins.

Fibre breakage of z-pins is mainly due to the axially tensile loading, instead of axially compressive loading. A classical two-parameter Weibull's failure criterion [17][18] is employed to evaluate the z-pin tensile strength based on each element by:

$$S_E = S_{ASTM} \cdot \left(\frac{V_{ASTM}}{V_E}\right)^{1/m} \quad (6)$$

where V_E is the volume of a z-pin element; V_{ASTM} and S_{ASTM} are the volume and tensile strength of standard ASTM sample. For numerical stability, a damage evolution (softening regime) is defined [19], following the point when element tensile strength is reached.

3. Model verification

At the first stage of model verification, the modelling strategy was used to predict the mode I high-rate bridging behaviour of a 4×4 T300/BMI composite z-pin array when inserted in a quasi-isotrpoic IM7/8552 laminate block. Experimental characterisation of the z-pinned laminate has been performed in [5]. The z-pin diameter is 0.28 mm. The full mesh of the z-pinned laminate is shown in Fig. 3. The laminate block is separated at the mid-plane and bridged only by the z-pin array. All the z-pins were assumed to show a through-thickness offset angle at 9° and have no in-plane offset, which were observed in actual specimens. Thus, a resin channel is formed between two adjacent z-pins in 0° and 90° plies, since they are aligned well and the pin to pin distance is smaller than the resin pocket length. The laminate was tested by a modified Split Hopkinson Bar (SHPB) set-up, which was also included in the FE model. As shown in Fig. 4, a striker bar traveling at an initial velocity hits the loading bar, thus generating a tensile pulse in the loading bar. The tensile pulse travels down to the input bar, which pulls out the z-pins via a custom-designed rig under a constant loading velocity. Table 1 lists the material properties used in the FE model. Table 2 lists the parameters used to define the ply-level meshes as shown in Fig. 2.

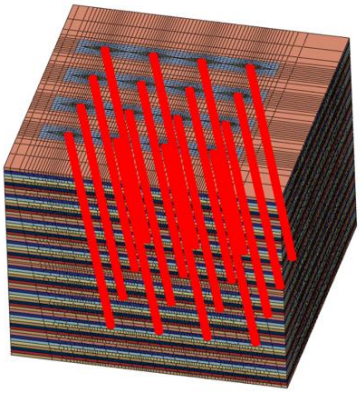

Figure 3. Finite element mesh of a 4×4 z-pin array reinforced laminate.

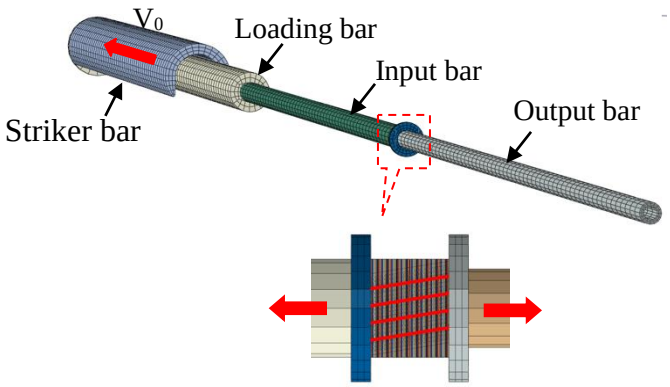

Figure 4. Full FE model of mode I high loading-rate test set-up for a z-pin array reinforced laminates.

Table 1. Material properties used in the FE model

Fibre		Resin epoxy		z-pin		z-pin/laminate interface	
E_1 (Ga)	276.0	E_1 (GPa)	4.6	E_1 (GPa)	144.0	K_I (N/mm)	36620
E_2 (Ga)	15.0	υ	0.35	E_2 (GPa)	7.31	K_{II} (N/mm)	13770
υ_{12}	0.2	υ_p	0.3	υ_{12}	0.25	σ_{max} (MPa)	6.37
G_{12} (Ga)	15.0	X_c (MPa)	65	G_{12} (Ga)	12.42	τ_{max} (MPa)	9.56
G_{23} (Ga)	7.0	X_t MPa)	180	G_{23} (GPa)	2.629	G_{cI} (N·mm)	0.16
VF_0	57.5%	G_{cI} (N·mm)	0.09	X_L (GPa)	1.86	G_{cII} (N·mm)	0.55
VF_{max}	70%	α_C	0.084	S_L (GPa)	0.12	μ	0.6
				G_{cI} (N·mm)	89.83	τ_0 (GPa)	5.42
				G_{cII} (N·mm)	1.0	δ_0 (mm)	0.01
				m	35		
				S_{ASTM}(GPa)	3750		
				A	138		
				B	45		

Table 2. Ply-level mesh definition parameters

L (mm)	2.0
W_{RP} (mm)	0.3
W (mm)	0.8

Fig. 5 shows the fibre volume distribution in a 0° ply. Fig. 6 compares the FE predicted and experimentally measured load-displacement curves under 5.5 m/s pullout. Two FE curves are given that were achieved by treating the z-pins with and without the nonlinear shear definition by Eq. 5, respectively. The z-pin becomes too compliant in the nonlinear shear model that the displacement at full pullout is much larger than half of the original pin insertion length. It means that the nonlinear shear parameters given in Table 1 are too low, thus a parameter study needs to be undertaken to find more reasonable values. The model with z-pin treated as an elastic material gave the correct displacement at full pullout. It also gave excellent prediction regarding the whole frictional pullout, however, the z-pin/laminate interface parameters need to be adjusted to achive satisfactory prediction regarding the interface debonding stage, mainly for the overall pullout stiffness and peak load at debonding.

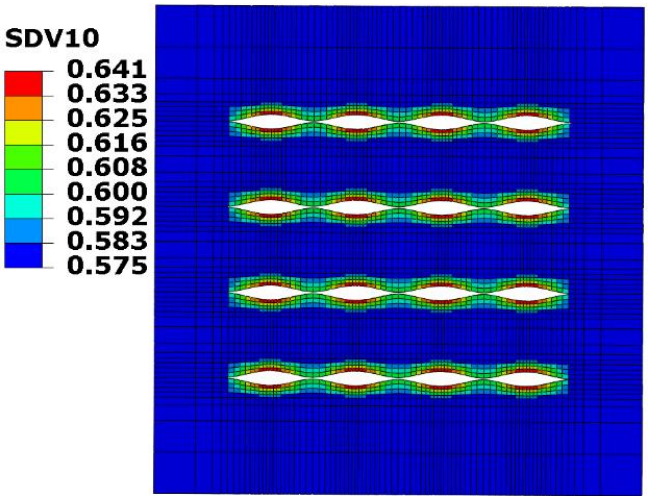

Figure 5. Fibre volume distribution in a 45° ply.

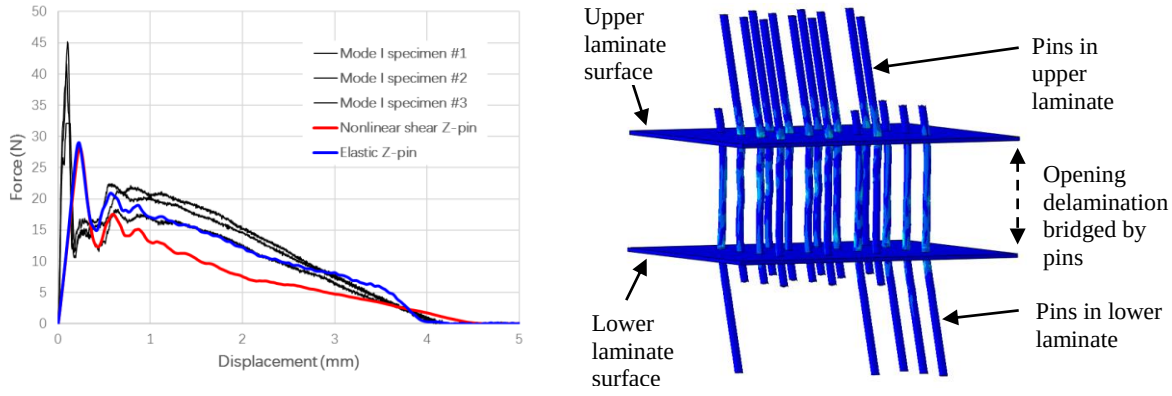

(a) (b)

Figure 6. (a) comparison between experimental and numerical load-displacement curves under (a) 5.5 m/s mode I pullout and (b) a snapshot capatured in the FE model

4. Conclusions

This work presents an advanced finite elemet model that can be used to investigate and understand the high-loading-rate bridging mechanisms of z-pins. It first introduced two ply-level meshes that can be used to describe 0° plies, 90° plies and ±45° plies, respectively. These ply-level meshes take into account the significant micro-mechanical features of z-pinned laminate, including the resin pocket (channel), fibre waviness around z-pins, fibre volume fraction variaton in the fibre waviness region and the z-pin misalignment. The z-pin/laminate interface is described by a cohesive-friction law, which applied a modified Coulomb friction law on the interface once damage is initiated. Z-pins were described by a nonlinear shear constitutive equation to consider the bending stiffness variation due to splitting and post-splitting frictional contact between split strands. A Weibull statistical failure criterion was used to govern the tensile rupture of z-pins.

The model has been preliminarily applied to simulate the mode I high-rate bridging behaviour of a 4 × 4 T300/BMI z-pin array when inserted in a quasi-isotropic carbon fibre laminate. The numerical model has successfully captured z-pin/laminte debonding and frictional pullout, however, further parametric studies need to be carried out to find out the optimum modelling parameters.

Acknowledgments

This research was conducted as a part of the EPSRC project, ‘Understanding Delamination Suppression at High Deformation Rates in Through-Thickness Reinforced Laminated Composites’ (Grant no. EP/M015319/1). The authors also thank their collaborator Dr. H Cui (Oxford University) for providing the experimental data used for model validation.

References

[1] A.P. Mouritz. Review of z-pinned composite laminates. *Composites Part A Applied Science and Manufacturing*, 38:2383–2397, 2007.

[2] A. Schlueter. An experimental study of rate effects on Mode I delamination of Z-pinned composite laminates. *Purdue University, PhD thesis*, 2012.

[3] X. Zhang, L. Hounslow, and M. Grassi. Improvement of low-velocity impact and compression-after-impact performance by z-fibre pinning. *Composites Science and Technology*, 66:2785–2794, 2006.

[4] M. Knaupp, F. Baudach, J. Franck, and G. Scharr. Impact and post-impact properties of cfrp laminates reinforced with rectangular z-pins. *Composites Science and Technology*, 87:218–223, 2013.

[5] M. Yasaee, G. Mohamed, A. Pellegrino, N. Petrinic, and S.R. Hallett. Strain rate dependence of mode II delamination resistance in through thickness reinforced laminated composites. *International Journal of Impact Engineering*, 107:1–11, 2017.

[6] H. Cui, M. Yasaee, G. Kalwak, A. Pellegrino, I.K. Partridge, S.R. Hallett, G. Allegri, and N. Petrinic. Bridging mechanisms of through-thickness reinforcement in dynamic mode I&II delamination. *Composites Part A Applied Science and Manufacturing*, 99:198–207, 2017.

[7] H. Cui, M. Yasaee, S.R. Hallett, I.K. Partridge, G. Allegri, and N. Petrinic. Dynamic Bridging Mechanisms of Through-Thickness Reinforced Composite Laminates in Mixed Mode Delamination. *Composites Part A Applied Science and Manufacturing*, 106:24–33, 2017.

[8] B. Zhang, G. Allegri, M. Yasaee, and S.R. Hallett. Micro-mechanical finite element analysis of Z-pins under mixed-mode loading. *Composites Part A Applied Science and Manufacturing*, 78:424–435, 2015.

[9] A.R. Melro, P.P. Camanho, F.M. Andrade Pires, and S.T. Pinho. Micromechanical analysis of polymer composites reinforced by unidirectional fibres: Part I-Constitutive modelling. *International Journal of Solids and Structures*, 50:1897–1905, 2013.

[10] X. Bai, M. A. Bessa, A.R. Melro, P.P. Camanho, L. Guo, and W.K. Liu. High-fidelity micro-scale modeling of the thermo-visco-plastic behavior of carbon fiber polymer matrix composites. *Composite Structures*, 134:132–141, 2015.

[11] A.R. Melro, H. Cui, N. Petrinic, I.K. Partridge, and S.R. Hallett. High-fidelity modelling of damage mechanisms in through-thickness reinforced composites. *Proceedings of the 21st International Conference on Composite Materials ICCM-21, Xi'an, China*, August 20-25 2017.

[12] G. Alfano and E. Sacco. Combining interface damage and friction in a cohesive-zone model. *International Journal for Numerical Methods in Engineering*, 68: 542–582, 2006.

[13] B. Zhang, G. Allegri, and S.R. Hallett. High-fidelity modelling of Z-pins in quasi-istropic laminates. *Proceedings of the 16th European Conference on Composite Materials ECCM-16, Seville, Sapin*, June 22-26, 2014.

[14] B.N. Cox and N. Sridhar. A traction law for inclined fiber tows bridging mixed-mode cracks. *Mechanics of Advanced Materials and Structures*, 9:299–331, 2002.

[15] B.N. Cox. Snubbing effects in the pullout of a fibrous rod from a laminate. *Mechanics of Advanced Materials and Structures*, 12: 85–98, 2005.

[16] S. Mukhopadhyay, M.I. Jones, and S.R. Hallett. Compressive failure of laminates containing an embedded wrinkle; Experimental and numerical study. *Composites Part A Applied Science and Manufacturing*, 73:132–142, 2015.

[17] M.R. Wisnom. Relationship between strength variability and size effect in unidirectional carbon fibre/epoxy. *Composites*, 22:47–52, 1991.

[18] X. Li, S.R. Hallett, and M.R. Wisnom. A finite element based statistical model for progressive tensile fibre failure in composite laminates. *Composites Part B: Engineering*, 45:433–439, 2013.

[19] P. Maimi, P.P. Camanho, J.A. Mayugo, and C.G. Dávila. A thermodynamically consistent damage model for advanced composites. *NASA Technical Reports*, NASA/TM-2, 2006.